Article:
Han, H-S, Lee, H, Lim, J et al. (2017) Hopping Conduction in (Ni,Co,Mn)O_4 Prepared by Different Synthetic Routes: Conventional and Spark Plasma Sintering. Ceramics International, 43 (18). pp. 16070-16075. ISSN: 0272-8842

https://doi.org/10.1016/j.ceramint.2017.08.105

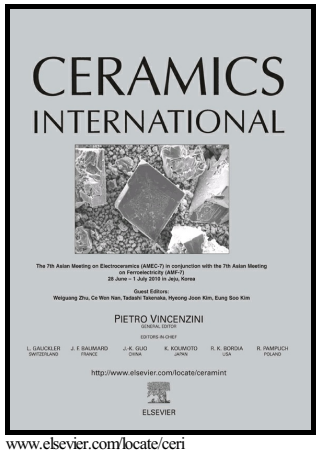

www.elsevier.com/locate/ceri

Hopping Conduction in $(Ni,Co,Mn)O_4$ Prepared by Different Synthetic Routes: Conventional and Spark Plasma Sintering

HyukSu Han, Hanchan Lee, Jiun Lim, Kang Min Kim, Yu-Rim Hong, Jaeseok Lee, Jennifer Forrester, Jeong Ho Ryu, Sungwook Mhin

PII: S0272-8842(17)31803-5
DOI: http://dx.doi.org/10.1016/j.ceramint.2017.08.105
Reference: CERI16059

To appear in: *Ceramics International*

Received date: 13 August 2017
Accepted date: 16 August 2017

Cite this article as: HyukSu Han, Hanchan Lee, Jiun Lim, Kang Min Kim, Yu-Rim Hong, Jaeseok Lee, Jennifer Forrester, Jeong Ho Ryu and Sungwook Mhin, Hopping Conduction in $(Ni,Co,Mn)O_4$ Prepared by Different Synthetic Routes: Conventional and Spark Plasma Sintering, *Ceramics International,* http://dx.doi.org/10.1016/j.ceramint.2017.08.105

Hopping Conduction in $(Ni,Co,Mn)O_4$ Prepared by Different Synthetic Routes: Conventional and Spark Plasma Sintering

HyukSu Han,[1] Hanchan Lee,[2] Jiun Lim,[3] Kang Min Kim,[2] Yu-Rim Hong,[1,4] Jaeseok Lee,[5] Jennifer Forrester,[6] Jeong Ho Ryu[7], Sungwook Mhin [1,*]

[1]Korea Institute of Industrial Technology, Gwahakdanji-ro 137-41, Gangwon-do, 25440, Republic of Korea

[2]Korea Institute of Industrial Technology, Gaetbeol-ro 156, Yeonsu-gu, Incheon, 406-840, Republic of Korea

[3]Department of Materials Science and Engineering, Ajou University, World cup-ro 206, Suwon-si, Gyeonggi-do, 443-749, Republic of Korea

[4]Department of Chemistry, Seoul Women's University, Seoul, Republic of Korea

[5]Department of Materials Science and Engineering, University of Florida, Gainesville, FL 32611, USA

[6]School of Chemical and Process Engineering, University of Leeds, Leeds, West Yorkshire, LS2 9JT United Kingdom

[7]Department of Materials Science and Engineering, Korea National University of Transportation, Chungju, 380-702, Republic of Korea

* Author to whom correspondence should be addressed.

Electronic mail: hyeleci@kitech.re.kr, Office: +82 31 8084 8641, Fax: +82 31 8084 8603

ABSTRACT

$(Ni,Co,Mn)O_4$ (NMC) oxides were prepared by conventional sintering (CS) and spark plasma sintering (SPS) using micro and nanopowders. Small hoping polaron theory was used in order to investigate effect of processing routes on electrical properties of NMC oxides as negative temperature coefficient (NTC) thermistors. Also, X-ray diffraction (XRD), scanning electron microscopy (SEM), and X-ray photoelectron spectroscopy (XPS) techniques were utilized to analyze compositional and structural effects on the electrical properties of NMC compounds. Hopping conduction in NMC prepared by SPS and CS using nanopowder occurs via variable range hopping (VRH) mechanism, however conduction in NMC prepared by CS using micropowder follows nearest neighboring hopping (NNH) mode. Hopping distance and activation energy for the VRH mode were calculated using corresponding physical model.

Keywords: Nickel cobalt manganese oxides, spinel, hopping conduction, nanopowder, spark plasma sintering, conventional sintering

INTRODUCTION

$(Ni,Co,Mn)O_4$ (NMC) oxides as a negative temperature coefficient (NTC) thermistor has been extensively studied for various applications such as temperature sensor devices, surge protection devices, and infrared detecting bolometers.[1-3] As a temperature sensor, important property of the NMC is exponentially decreasing resistance with increasing temperature, which is described by following equation;

$$R = R_0 \cdot \exp\left(\frac{E_a}{k \cdot T}\right) = R_0 \cdot \exp\left(\frac{B}{T}\right) \quad (1)$$

$$B = \frac{T_1 \cdot T_2}{T_2 - T_1} \cdot \ln\left(\frac{R_1}{R_2}\right) \quad (2)$$

where B is the thermal sensitivity factor which is closely related to the activation energy for hopping conduction (E_a). Also, R, k and T are resistance, the Boltzmann constant and absolute temperature, respectively.

Generally, NMC oxide is prepared via conventional solid-state-reaction route which requires extremely high firing temperature up to 1400°C and long sintering time up to 10 h. In the conventional sintering (CS) process, phase transition from cubic to tetragonal structure during cooling is inevitable for NMC compounds.[4, 5] The phase transition in NMC causes several issues for the application of NTC thermistor; microcracks, phase separation, and secondary phase formation. Among these, microcracks in the sintered body, which is induced by volume difference between cubic and tetragonal phases, is directly related to the reliability of the

fabricated NTC thermistors. Thus, search for alternative sintering processing route which can suppress phase transition in NMC compounds is necessary.

Spark plasma sintering (SPS) is a fast-firing sintering process where high amplitude of current (>1000 Amp) at a low voltage (5 V) is applied to powder compact.[6, 7] The resistive heating thanks to high amplitude of direct current leads to a rapid temperature rise within the powder compact. Thus, the powder can be sintered at significantly lower temperature in a shorter period of time compared to CS process. Therefore, the phase transition of NMC compounds during cooling from the elevated temperature can be avoidable, when SPS technique is adapted for sintering process. Additionally, SPS is conducted under vacuum which can facilitate the formation of oxygen vacancies combined with the reduction of cations in the NMC oxide.

Small polaron hopping model is commonly proposed for the electrical conduction of the NMC.[8, 9] Hopping conduction in spinel compounds is significantly influenced by the oxygen content and the cation distributions on the different crystallographic sites which are very sensitive to sample preparation methods.[8, 10] The reduction of cations can be boosted when nanopowder is used as starting materials due to the high surface area to volume ratio.[10, 11] As more charge balance of cations are uncompensated, cation distribution in the NMC can be significantly disturbed leading to unique charge transfer mechanism in the compound.

In this work, we prepared NMC ceramics using NMC nanopowder combined with SPS sintering process (SPS NP) to obtain single cubic phase with disturbed cation distributions. Compositional and structure analysis were performed on SPS NP ceramics using appropriate techniques such as X-ray diffraction (XRD), scanning electron microscopy (SEM) and X-ray photoelectron spectroscopy (XPS). Furthermore, in-depth analysis on charge transfer mechanism

in the SPS NP compound is conducted using small polaron hopping theory and the corresponding hopping conduction model is proposed.

EXPERIMENTAL PROCEDURE

NMC naopowder (NMC NP) was synthesized by auto-combustion method using manganese (II) nitrate ($Mn(NO_3)_2$; 50% aqueous solution), Cobalt (II) nitrate hexahydrate ($Co(NO_3)_6 \cdot H_2O$), Nickel (II) nitrate hexahydrate ($Ni(NO_3)_6 \cdot H_2O$), and citric acid as starting materials. Stoichiometric amounts of $Mn(NO_3)_2$, $Co(NO_3)_{26}H_2O$, $Ni(NO_3)_{26}H_2O$, and citric acid were dissolved in distilled water. The molar ratio of nitrate to citric acid was 1:1. Ammonia was dropped into the solutions to change pH value from 1 to 6. The solution was heated at 80 °C to transform to sol followed by heating at 130 °C under constant stirring for the formation of brownish gel. Processing temperature for the formation of sol and gel was measured by infrared thermometer (AR 500, Smart sensor®, China). Subsequently, gel was heated at 300 °C until all the gel was completely burnt out for the formation of fine powder. The prepared powder was calcined at 700 °C with a heating rate of 5 °C /min for 2 h under air. More information relating with preparation of NMC NP is available in our previous paper.[4, 5]

Prepared NMC NP was sintered via two different sintering technique; CS and SPS. For CS, NMC NP prepared by auto combustion method was pressed to prepare pellets of 1 mm-thick and 2 cm in diameter and then, sintered at 1200 °C for 8 h with heating rate of 5°C/min and subsequently, cooled down naturally to room temperature. For SPS, NMC NP prepared by auto combustion method was introduced to graphite die with the internal diameter of 25 mm. The powder was then sintered under 50 MPa for 5 min between 700 °C and 750 °C with heating rate

of 50 °C/min using Dr. Sinter (SPS-625, SPS Syntex Inc., Japan). After sintering, both side of the prepared pellets were polished to remove the (Mn, Co)O_x reduced phase.

Diffraction patterns of NMC oxides prepared by different processing method were recorded using Panalytical X'pert–pro MPD with CuKα radiation. Microstructure and elemental mapping of Ni, Co and Mn at the NMC oxides were investigated using scanning electron microscopy (SEM; Nova NanoSEM, FEI, USA) equipped with energy-dispersive X-ray (EDX) spectroscopy. Also, oxidation states of Ni, Mn and Co were analyzed using X-ray Photoelectron Spectroscopy (XPS; ESCALAB 250xi, thermoscientific, USA). Resistivity as a function of temperature in the range of 25 °C and 80 °C was measured using LCR meter (IM3570, Hioki, Japan).

RESULTS AND DISCUSSION

XRD patterns of the NMC oxides prepared by different processing routes are shown in **Figure. 1**. XRD patterns for the prepared pellets via CS using NMC nanopowder (CS NP) and micropowder (CS MP) are also shown for the comparison purpose. XRD pattern of CS MP shows the mixed phase with cubic and tetragonal spinel structure. As we previously reported, cubic spinel structure is thermodynamically stable at NMC oxides over 1000 °C at heating and then, gradually transforms to tetragonal spinel during cooling a as confirmed by *in situ* XRD study.[4] As far as high temperature (~1200 °C) and comparatively long sintering time are required to sinter NMC, the phase transformation from cubic to tetragonal spinel is unavoidable. Also, the formation of CoO as a secondary phase can occur due to the phase decomposition of NMC during sintering at high temperature above 1200 °C. It can be attributed to the reduction of NMC oxides at high temperature. For CS NP, although the secondary phase of CoO was disappeared, the mixture of cubic and tetragonal phases is still existed. However, when SPS was

applied with NMC NP (i.e., SPS NP), XRD pattern clearly shows the cubic spinel structure ($Fd\bar{3}m$; JCPDS card No. 23-1237) without any secondary phases. It indicates that the cubic spinel structure of the NMC retained without formation of secondary phases owing to fast quenching from lower sintering temperature (~700 $^{\circ}$C). Thus, sintering of NMC NP at lower temperature combined with fast quenching can prohibit the phase transformation of cubic spinel to tetragonal spinel during cooling resulting in phase pure cubic spinel structure.

Microstructure of the NMC pellets prepared via different routes is shown in **Figure. 2**. Grain sizes between 1 um and 10 um were observed at both CS MP and NP, while grain size below 100 nm was observed SPS NP implying that SPS can prohibit grain growth due to shorter sintering time at lower temperature. Also, mechanical loading for the pellet during SPS leads to the formation of more dense pellets. Element mapping results confirm homogeneous distribution of Ni, Co and Mn indicating no phases segregation during sintering process.

XPS spectra of Ni, Co and Mn for NMC samples are shown in **Figure. 3**. For all samples, Mn 2p spectra features strong spin-orbit peaks of the $2p_{3/2}$ and $2p_{1/2}$ centered at 642 eV and 654 eV, respectively. Each peak of Mn2p can be deconvoluted into two characteristic peaks which assigned to Mn^{3+} and Mn^{4+}, respectively, implying that Mn^{3+} and Mn^{4+} coexist.[12] Similarly, mixed valence of Co^{2+} and Co^{3+} was observed at Co 2p spectra of all samples.[13-15] Co 2p spectra shows two major peaks at 780 eV and 795 eV, which can be assigned to Co $2p_{3/2}$ and Co $2p_{1/2}$ energy levels. Given that the spin orbit splitting for the Co 2p is approximately 15 eV.[15] Also, shake-up satellite peaks centered at 788eV and 802eV confirmed the presence of Co^{3+} in Co $2p_{3/2}$ and Co $2p_{1/2}$ states, respectively. All major and satellite peak may be able to be deconvoluted into two characteristic curves, indicating the presence of Co^{2+} cations in NMC

compounds. In the Ni 2p spectra, $Ni2p_{3/2}$ and $Ni2p_{1/2}$ centered at 855 eV and 873 eV were observed with the corresponding two satellite peaks near at 861 eV and 880 eV, respectively.[16] This indicates the existence of Ni^{2+}. XPS data shows that NMC pellets prepared via different routes is consisted of cations with mixed-valence states where oxidation states of the Ni ions are 2+, whereas Mn and Co ions are 3+/4+ and 2+/3+, respectively.

Electrical properties of CS MP, CS NP, and SPS NP are investigated. As shown in **Figure. 4**, semiconductive properties are observed for all samples; resistivity exponentially decreases as increasing temperature, which is a typical R-T curve of NTC thermistors. CS MP exhibits the room temperature resistance of 92,548 Ω (**Figure. 4**), while CS NP and SPS NP show much smaller resistance at room temperature, 667.3 and 914.9 Ω, respectively. Also, as can be seen in **Figure 5**, B-values for CS NP (3,408 K) and SPS NP (3,495 K) was much larger than that of CS MP (3,280 K).

In order to investigate the electrical conduction mechanism of NMC samples, small polaron hopping theory is applied. Hopping conduction in spinel oxide can be explained as macroscopic percolation system consisting of a random resistor network.[9] Two contributions of spatial and energy terms compete each other to determine a percolation threshold, which is written as follows;

$$\xi_c \geq \xi_{ij} = \frac{2r_{ij}}{a} + \frac{\varepsilon_{ij}}{k_B T} \qquad (3)$$

where r_{ij} and ε_{ij} are the separation of the i and j electrons in real and energy space, respectively. k_B is the Boltzman constant and a is a localization length which can be assumed as ionic radii of Mn^{3+} for spinel manganese. The relative contribution of two terms determines whether hopping

occurs within the nearest neighbors or not, which are referred to as nearest neighboring hopping (NNH) and variable range hopping (VRH), respectively. NNH and VRH models can be described by the following equation,

$$\rho(T) = CT^{\alpha} \exp\left(\frac{T_0}{T}\right)^{p} \quad (4)$$

where C and T_0 are a constant and characteristic temperature, respectively. For NNH, since r_{ij} is constant, T_0 is only proportional to ε_{ij} with $\alpha = p = 1$. In the case of VRH, $\alpha = 2p$ and T_0 is associated with the shape of the density of states (DOS) at the Fermi level, p values can be 1/4 and 1/2 when DOS has uniform and parabolic shapes around the Fermi level, respectively.[17] According to Shklovskii and Efros, p value can be obtained by calculating the slope of a ln(W)-ln(T) plot [9, 17]:

$$W = \frac{1}{T}\frac{d(\ln\rho)}{d(T^{-1})} \approx -p\left(\frac{T_0}{T}\right)^{p} \quad (5)$$

Figure 6 shows the calculated p-values for NMC samples using the 1st derivative of the R-T data. p values were determined as 0.53, 0.63, and 0.9 for SPS NP, CS NP, and CS MP, respectively. This result implies that conduction occurs by VRH mode for SPS NP and CS NP, while NNH mode prevails hopping conduction in CS MP, implying that CoO phase might have significant effect on altering hopping conduction mechanism in NMC phase. **Figure. 7** represents ρ – T data of the NMC samples plotted by following VRH (p value = 1/2) for SPS NP and CS NP, and NNH (p value =1) mode for CS MP, respectively. As can be seen in **Figure. 7**, a good linearity was observed in ln(ρ) vs. 1/T plot of CS MP, verifying that hopping conduction proceeds via NNH for CS MP. For CS NP, the average characteristic temperatures (T_0) was

calculated as 3,600 K, which corresponds to the activation energy of NNH conduction ($E_{A,NNH,}$ $T_0 = E_{A,NNH}/k_B$) of 0.33 eV. In contrast, For SPS NP and CS NP, ln(ρ) shows a good linearity when it plotted verses $1/T^{0.5}$, indicating the hopping conduction via VRH mode with the uniform DOS near the Fermi level for SPS NP and CS NP. As we suggested in our previous work, transition of hopping mode from VRH to NNH leads to huge increase of the room temperature resistance accompanied by huge drop of B value in spinel compound.[8] Thus, NNH hopping conduction in CS MP is responsible for high value of the room temperature resistance as well as low B value compared with those of SPS NP and CS NP. It is generally accepted that, compared to micropowder, nanopowder suffers from much more substantial reduction/oxidation when temperature changes due to high surface to volume ratio. As a result, high concentration of uncompensated charge balances can exist in the SPS NP and CS NP, which can act as available hopping sites for polarons. These hopping sites with high concentration may result in VRH conduction mode in SPS NP and CS NP.

In VRH conduction mode, activation energy as well as hopping distance may vary as a function of temperature.[10, 17-19] To calculate hopping distance as a function of temperature, the DOS at the vicinity of Fermi level (g') need to be obtained, and g' is related with the characteristic temperature ($T_{0)}$ as,

$$T_0 = \frac{1}{k_B}\left(\frac{21.2}{a^3 g'}(z+1)\right)^{1/(z+1)} \quad (6)$$

where z is associated with p value as p = (z+1)/(z+4) and *a* can be assumed as the Mn^{3+} cation radii (~0.7 Å) from a hard sphere model.[9] Then, hopping distance and activation energy for

VRH conduction ($E_{A.VRH}$) are determined at different temperature by using the following equations.[18]

$$R = a^{1/4} / [8\pi g' k_B T]^{1/4} \quad (7)$$

$$E_{A,VRH} = 0.5 k_B T_0^{0.5} T^{0.5} \quad (8)$$

Figure. 8 shows hopping distance and activation energy for SPS NP and CS NP as a function of temperature. It can be seen that for SPS NP, R decreases from 0.22 to 0.21 nm and $E_{A,VRH}$ increases from 0.32 to 0.35 eV as temperature increases from 300 to 350 K. Also, for CS NP, R decreases from 0.21 to 0.20 nm and $E_{A,VRH}$ increases from 0.30 to 0.33 eV at the same temperature range. The NNH and VRH parameters for NMC samples such as the resistivity at 303 K (ρ_{RT}), g', T_0, $E_{A,NNH}$, hopping distance at 303 K (R_{RT}), and $E_{A@RT,VRH}$ are summarized in **Table 1**. Compared to CS NP, SPS NP shows slightly higher B value which can be attributed to the single cubic spinel phase. Furthermore, longer hopping distance as well as larger activation energy of SPS NP for hopping conduction should be beneficial for improving B value, since polarons with larger hopping distance can have higher probability to be hopped to different sites securing higher number of conduction paths.

CONCLUSION

$(Ni,Co,Mn)O_4$ (NMC) samples were prepared using different processing routes including conventional sintering (CS) and spark plasma sintering (SPS) with different starting powders (microsize powder (MP) and nanopowders (NP)). X-ray diffraction (XRD) data verifies that CS MP and CS NP have mixture phase of tetragonal and cubic with secondary phase of CoO, while SPS NP is crystallized in pure cubic phase. Scanning electron microscopy (SEM) shows that SPS

NP has a much smaller grain size than CS NP and CS MP possibly due to shorter sintering time. Oxidation states of the cations such as Ni, Co, and Mn in NMC samples are analyzed by using X-ray photoelectron spectroscopy (XPS). XPS results demonstrate that all NMCs regardless of processing routes possess cations with mixed valence states. For electrical properties, SPS and CS NP show higher B value (3495 and 3408 K) and lower room temperature resistivity (667.3 and 914.9 Ω) compared to those of CS MP (3280 K, 92,548 Ω). Small polaron hopping theory predicts that hopping conduction in SPS NP and CS NP occurs via variable range hopping (VRH) mechanism while nearest neighboring hopping (NNH) prevails hopping conduction in NMC via CS MP. These results highlights significantly important role of CoO phase in determining electrical properties of NMC compound. In addition, bases on the calculated VRH parameters, higher B value of SPS NP compared to CS NP can be attributed to longer hopping distance and larger activation energy at different temperature.

ACKNOWLEDGEMENT

Authors want to acknowledge Hosang Chun for helpful discussion on this manuscript. This work was supported by the "Energy Efficiency & Resources" of the Korea Institute of Energy Technology Evaluation and Planning (KETEP) grant funded by the Korea government Ministry of Knowledge Economy (No. 20125010100030-11-2-400).

REFERENCE

[1] M. Vakiv, O. Shpotyuk, O. Mrooz, I. Hadzaman, Controlled thermistor effect in the system CuxNi1-x-yCo2yMn2-yO4, J Eur Ceram Soc, 21 (2001) 1783-1785.

[2] Z.B. Wang, C.H. Zhao, P.H. Yang, A.J.A. Winnubst, C.S. Chen, X-ray diffraction and infrared spectra studies of FexMn2.34-xNi0.66O4 ($0 < x < 1$) NTC ceramics, J Eur Ceram Soc, 26 (2006) 2833-2837.

[3] J.L. Tissot, IR detection with uncooled sensors, Infrared Phys Techn, 46 (2004) 147-153.

[4] S. Mhin, H. Han, D. Kim, S. Yeo, J.I. Lee, J.H. Ryu, Phase evolution of (Ni, Co, Mn)O-4 during heat treatment with high temperature in situ X-ray diffraction, Ceram Int, 42 (2016) 5412-5417.

[5] S. Mhin, H. Han, K.M. Kim, J. Lim, D. Kim, J.I. Lee, J.H. Ryu, Synthesis of (Ni,Mn,Co)O-4 nanopowder with single cubic spinel phase via combustion method, Ceram Int, 42 (2016) 13654-13658.

[6] D.M. Hulbert, A. Anders, J. Andersson, E.J. Lavernia, A.K. Mukherjee, A discussion on the absence of plasma in spark plasma sintering, Scripta Mater, 60 (2009) 835-838.

[7] S. Yoon, J. Dornseiffer, Y. Xiong, D. Gruner, Z.J. Shen, S. Iwaya, C. Pithan, R. Waser, Spark plasma sintering of nanocrystalline BaTiO3-powders: Consolidation behavior and dielectric characteristics, J Eur Ceram Soc, 31 (2011) 1723-1731.

[8] H. Han, J.S. Lee, J.H. Ryu, K.M. Kim, J.L. Jones, J. Lim, S. Guillemet-Fritsch, H.C. Lee, S. Mhin, Effect of High Cobalt Concentration on Hopping Motion in Cobalt Manganese Spinel Oxide (CoxMn3-xO4, x >= 2.3), J Phys Chem C, 120 (2016) 13667-13674.

[9] R. Schmidt, A. Basu, A.W. Brinkman, Small polaron hopping in spinel manganates, Phys Rev B, 72 (2005).

[10] H.S. Han, C. Davis, J.C. Nino, Variable Range Hopping Conduction in BaTiO3 Ceramics Exhibiting Colossal Permittivity, J Phys Chem C, 118 (2014) 9137-9142.

[11] H. Han, D. Ghosh, J.L. Jones, J.C. Nino, Colossal Permittivity in Microwave-Sintered Barium Titanate and Effect of Annealing on Dielectric Properties, J Am Ceram Soc, 96 (2013) 485-490.

[12] Z.M. Huang, W. Zhou, C. Ouyang, J. Wu, F. Zhang, J.G. Huang, Y.Q. Gao, J.H. Chu, High performance of Mn-Co-Ni-O spinel nanofilms sputtered from acetate precursors, Sci Rep-Uk, 5 (2015).

[13] Y. Wakisaka, S. Hirata, T. Mizokawa, Y. Suzuki, Y. Miyazaki, T. Kajitani, Electronic structure of Ca3Co4O9 studied by photoemission spectroscopy: Phase separation and charge localization, Phys Rev B, 78 (2008).

[14] F. Munakata, H. Takahashi, Y. Akimune, Y. Shichi, M. Tanimura, Y. Inoue, R. Itti, Y. Koyama, Electronic state and valence control of LaCoO3: Difference between La-deficient and Sr-substituting effects, Phys Rev B, 56 (1997) 979-982.

[15] C.C. Fu, G.S. Li, D. Luo, X.S. Huang, J. Zheng, L.P. Li, One-Step Calcination-Free Synthesis of Multicomponent Spinel Assembled Microspheres for High-Performance Anodes of Li-Ion Batteries: A Case Study of MnCo2O4, Acs Appl Mater Inter, 6 (2014) 2439-2449.

[16] J. Zhang, T. Wang, D. Pohl, B. Rellinghaus, R.H. Dong, S.H. Liu, X.D. Zhuang, X.L. Feng, Interface Engineering of MoS2/Ni3S2 Heterostructures for Highly Enhanced Electrochemical Overall-Water-Splitting Activity, Angew Chem Int Edit, 55 (2016) 6701-6706.

[17] R. Schmidt, A. Basu, A.W. Brinkman, Z. Klusek, P.K. Datta, Electron-hopping modes in NiMn2O4+delta materials, Appl Phys Lett, 86 (2005).

[18] H. Zheng, W.J. Weng, G.R. Han, P.Y. Du, Colossal Permittivity and Variable-Range-Hopping Conduction of Polarons in Ni0.5Zn0.5Fe2O4 Ceramic, J Phys Chem C, 117 (2013) 12966-12972.

[19] L. He, Z.Y. Ling, Studies of temperature dependent ac impedance of a negative temperature coefficient Mn-Co-Ni-O thin film thermistor, Appl Phys Lett, 98 (2011).

FIGURES

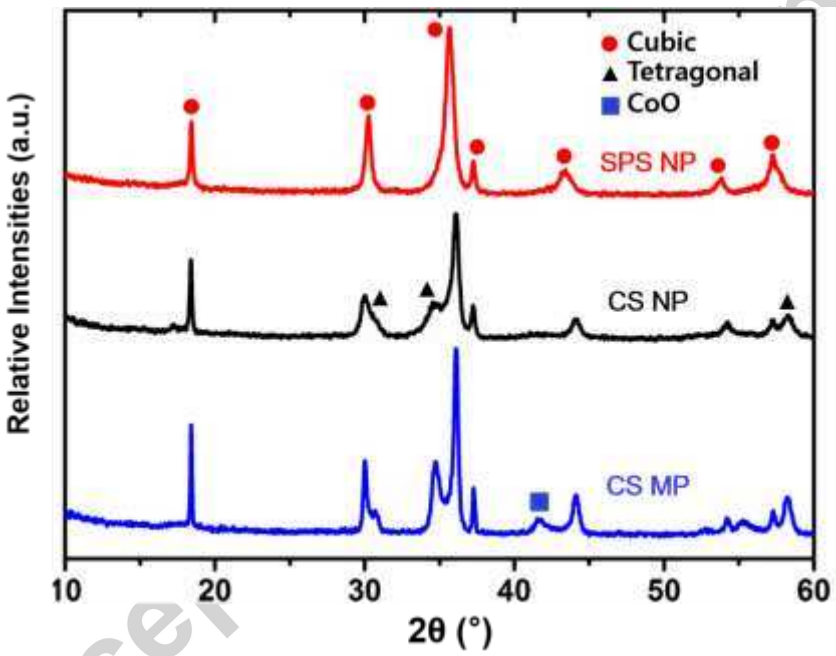

Figure 1. XRD patterns of the NMC oxides, CS MP (blue), CS NP (black), and SPS MP (red).

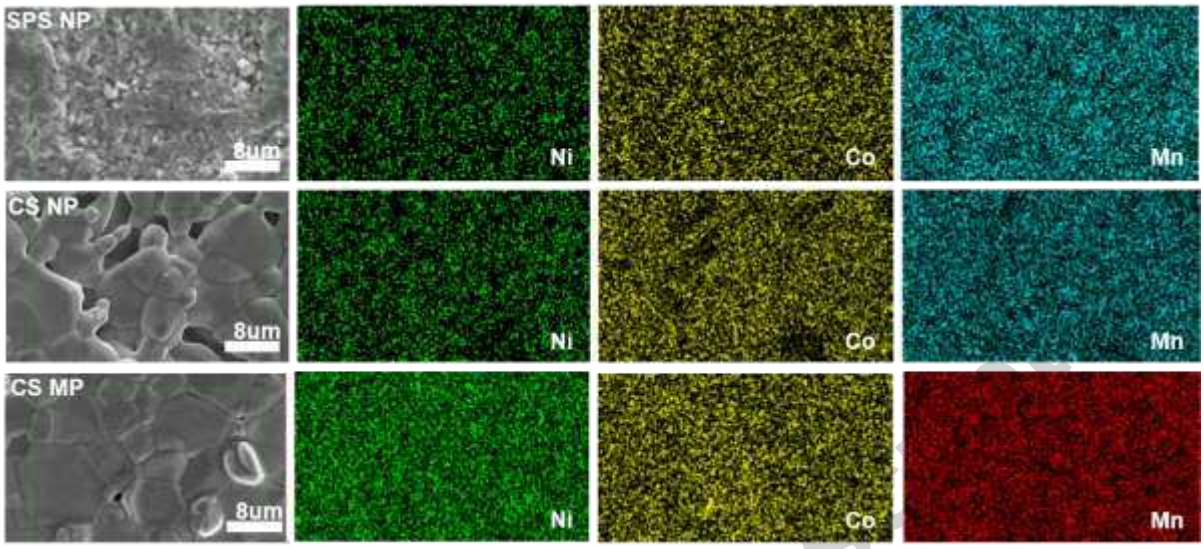

Figure 2. SEM image of SPS NP, CS NP, and CS MP with EDX elemental mapping results for Ni, Co, and Mn, respectively.

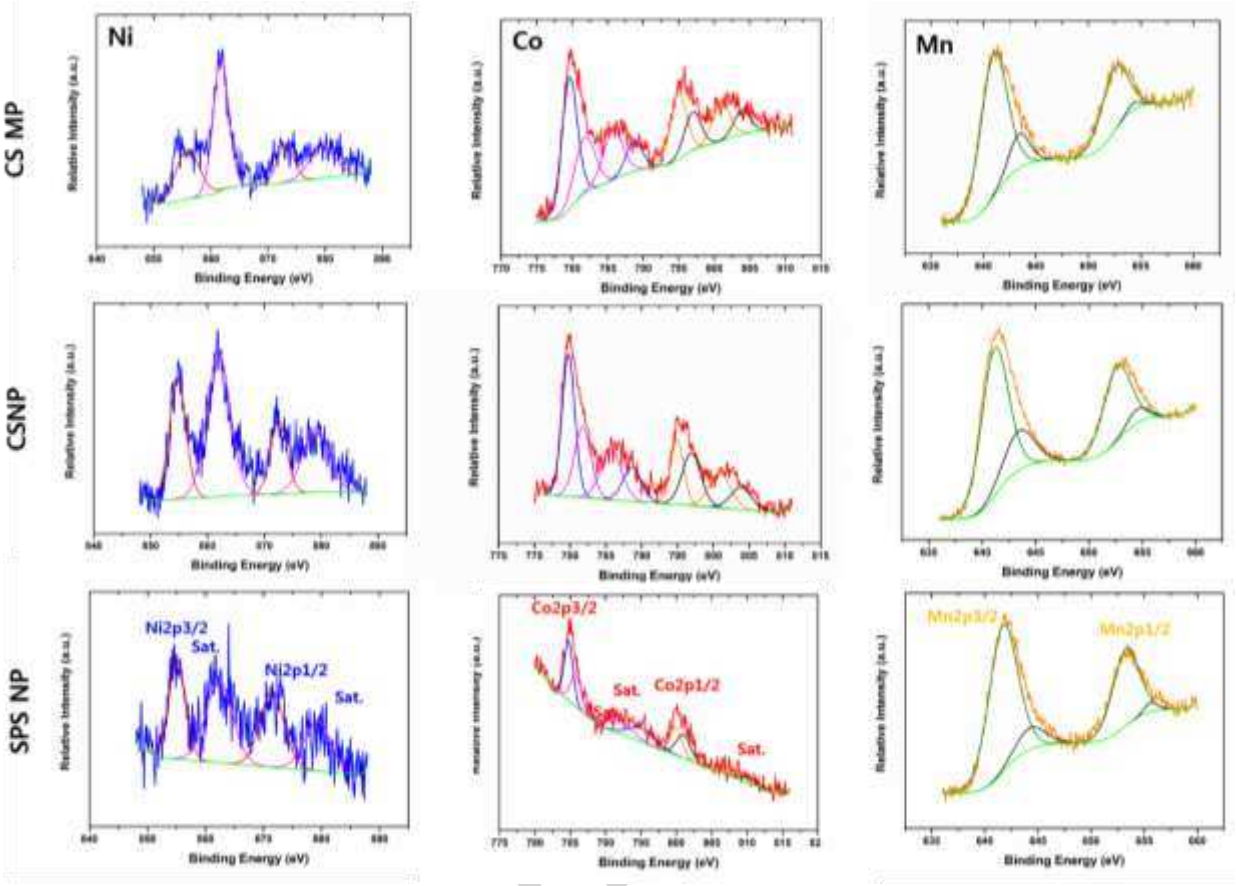

Figure 3. XPS spectra of SPS NP, CS NP, and CS MP for Ni 2pp, Co 2p, and Mn 2p orbitals with fitted lines.

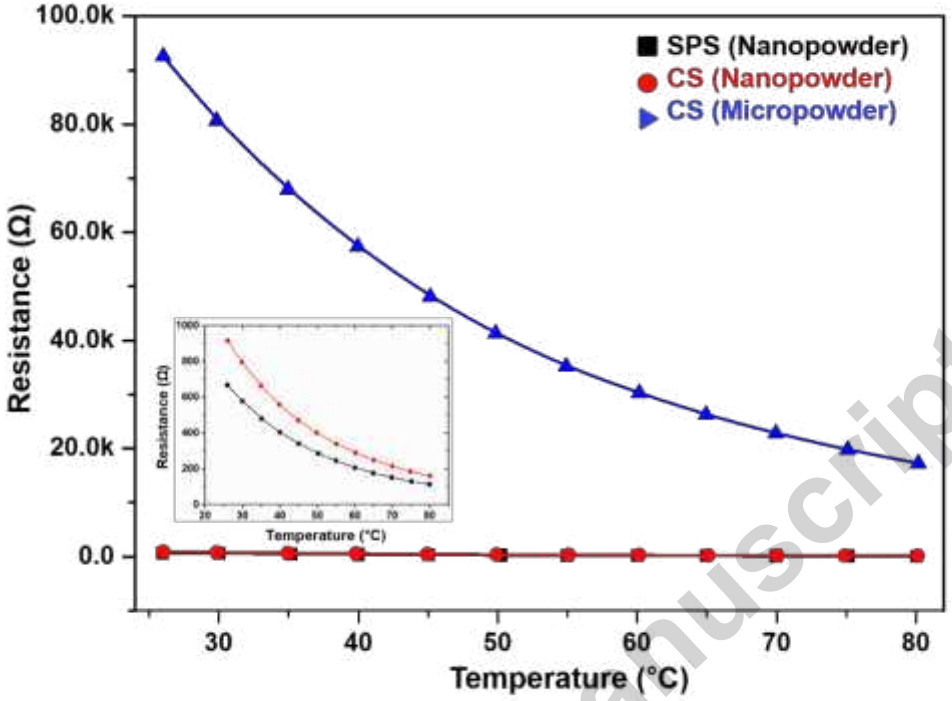

Figure 4. DC resistance versus temperature plots of NMC samples for the temperature range from 25℃ to 80℃.

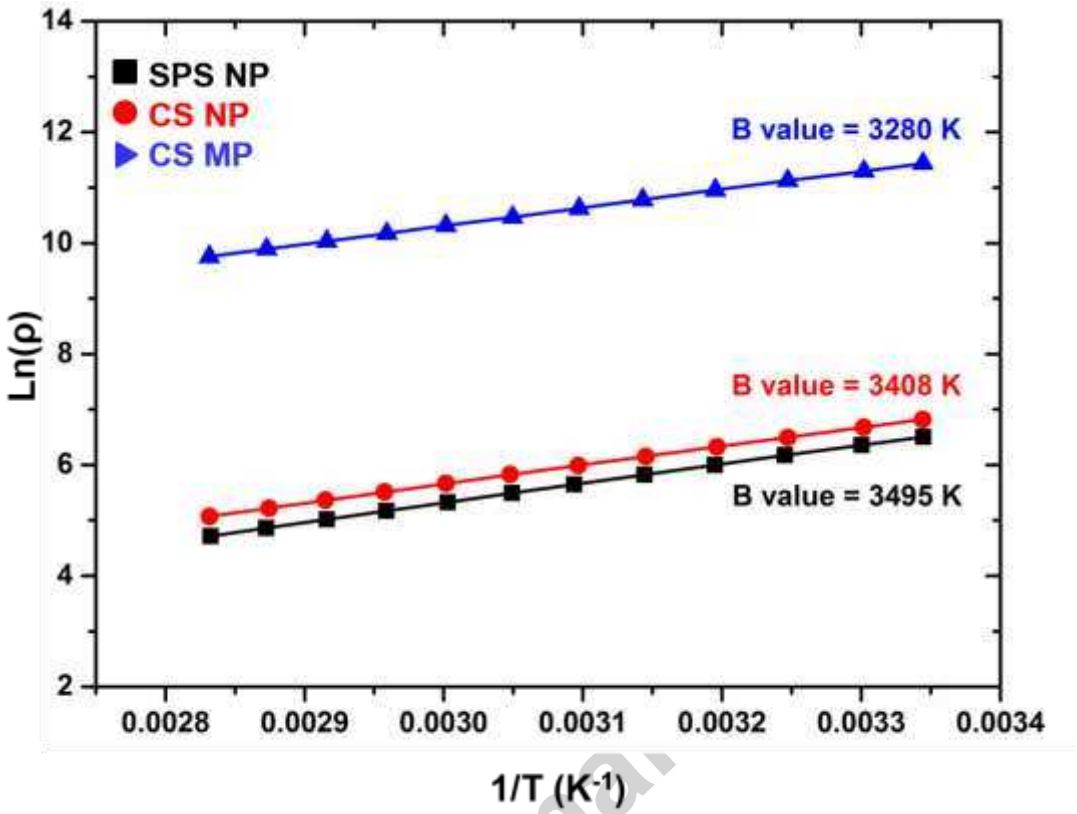

Figure 5. ln(ρ) vs. 1/T plots for NMC samples and the calculated B values.

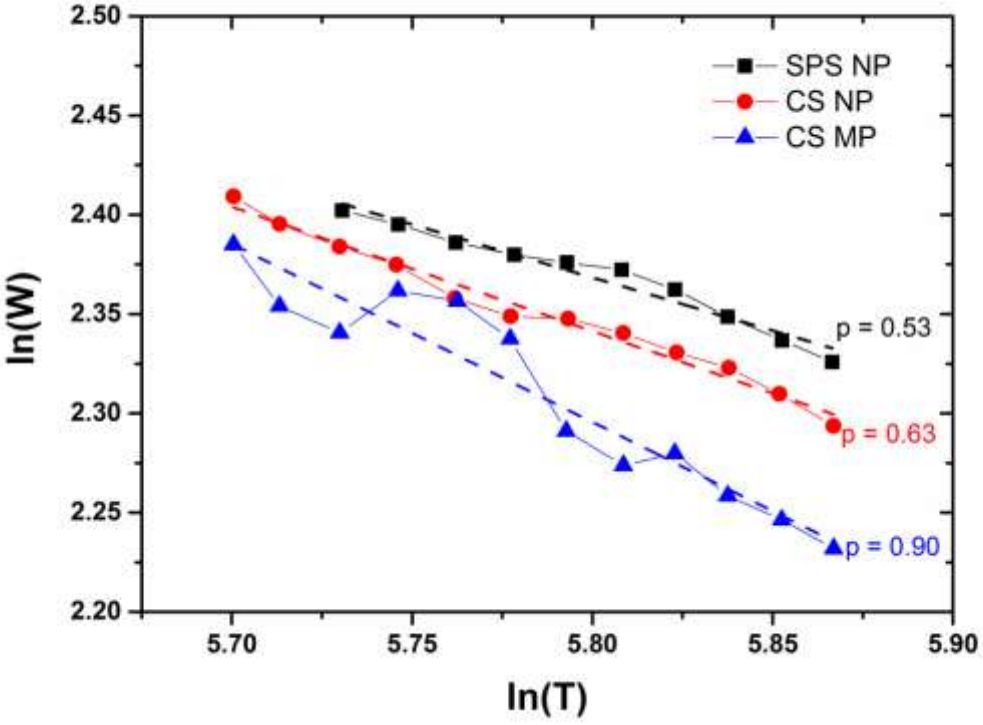

Figure 6. Calculated p values for SPS NP, CS NP, and CS MP, respectively.

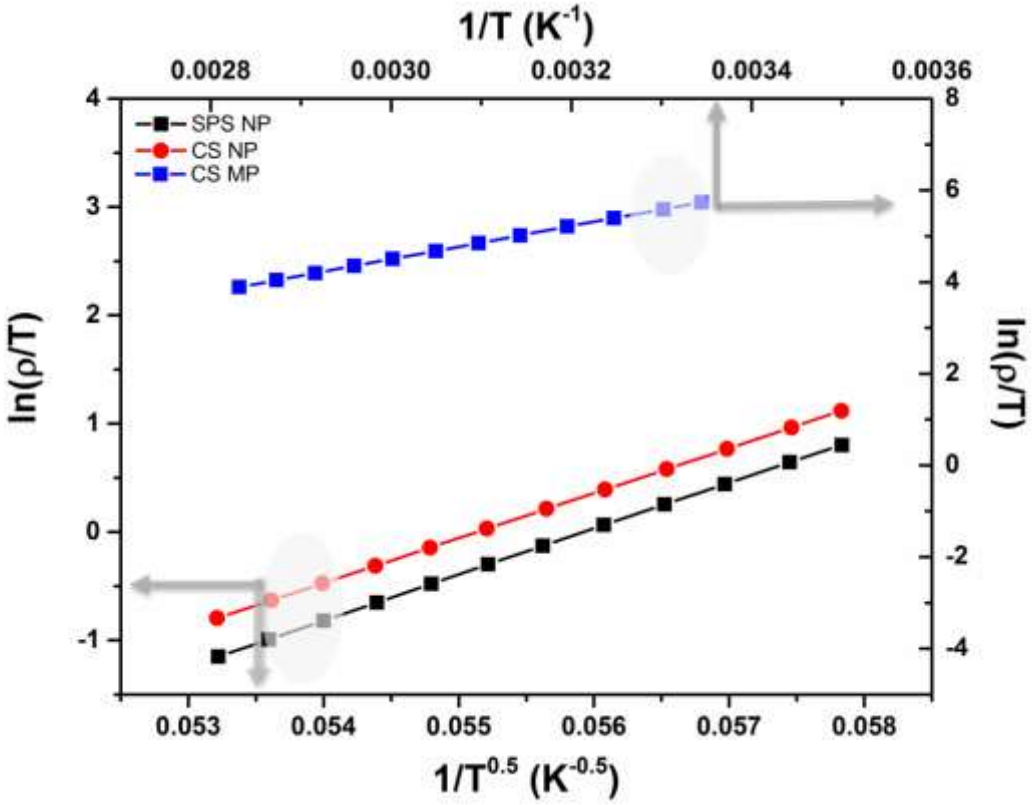

Figure 7. Plot of ln(ρ/T) vs. 1/T for CS MP and ln(ρ/T) vs. $1/T^{0.5}$ for SPS NP and CS NP.

.

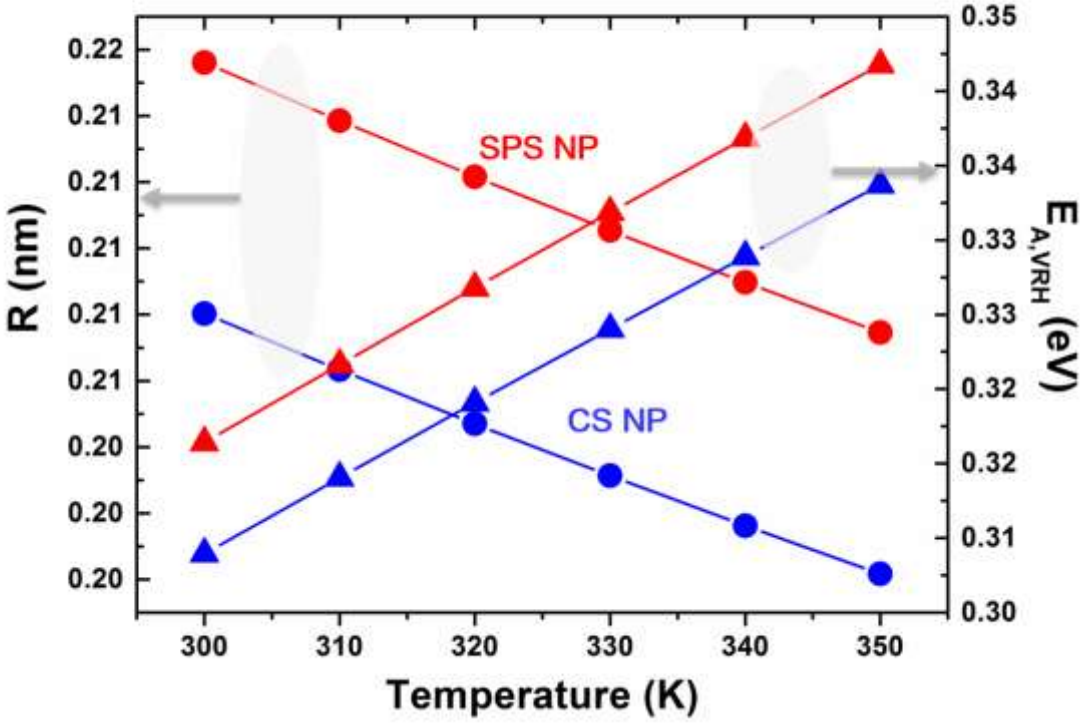

Figure 8. Hopping distance and activation energies as a function of temperature for SPS NP and CS NP following VRH conduction.

Table 1. ρ_{RT} and T_0 values for NMC samples. The calculated activation energy of NNH conduction ($E_{A,NNH}$) for CS MP sample. The calculated values of g', g(0.14eV), hopping distance ($R_{RT,}$ at room temperature), and activation energies of hopping conduction ($E_{A@RT,VRH}$, at room temperature) for SPS NP and CS NP samples following VRH motion.

	SPS NP	CS NP	CS MP
ρ_{RT} $(\Omega \cdot cm)$	667.3	914.9	92548.2
T_0 (K)	1.79×10^5	1.71×10^5	3.6×10^3
$E_{A,NNH}$ (eV)	N/A*	N/A	0.31
g' $(cm^{-3} \cdot eV^{-3})$	4.98×10^{22}	5.7×10^{22}	N/A
g(0.16eV) $(cm^{-3} \cdot eV^{-1})$	1.27×10^{21}	1.47×10^{21}	N/A
R_{RT} (nm)	0.21	0.20	N/A
$E_{A@RT,VRH}$ (eV)	0.31	0.30	N/A